N O T I C E

THIS DOCUMENT HAS BEEN REPRODUCED FROM MICROFICHE. ALTHOUGH IT IS RECOGNIZED THAT CERTAIN PORTIONS ARE ILLEGIBLE, IT IS BEING RELEASED IN THE INTEREST OF MAKING AVAILABLE AS MUCH INFORMATION AS POSSIBLE

9950 - 458

(NASA-CR-163888) EVALUATION OF HIGH SPECIFIC-HEAT CERAMIC FOR REGENERATOR USE AT TEMPERATURES BETWEEN 2-30 K Final Report (Lake Shore Cryotronics, Inc.) 39 p HC A03/MF A01 CSCL 11B G3/27

N81-16240

Unclas 41194

FINAL REPORT

JPL Contract No. 955446

EVALUATION OF HIGH SPECIFIC-HEAT CERAMIC FOR REGENERATOR USE AT TEMPERATURES BETWEEN 2-30 K

This work was performed for the Jet Propulsion Laboratory, California Institute of Technology, sponsored by the National Aeronautics and Space Administration under Contract NAS7-100.

Lake Shore Cryotronics, Inc.

Home Office
64 E. Walnut St. • Westerville, Ohio 43081 • (614) 891-2243 • Telex 24-5415 Cryotron WTVL
West Regional Office Sales & Service
4422 Macdonald Ave. • Suite 5 • Richmond, Ca. 94805 • (415) 237-9914

• *Cryogenic Thermometry* • *Instrumentation* • *Accessories*
• *Calibration Services* • *Engineering*
• *Systems*

FINAL REPORT

JPL Contract No. 955446

EVALUATION OF HIGH SPECIFIC-HEAT CERAMIC FOR REGENERATOR USE AT TEMPERATURES BETWEEN 2-30 K

W. N. Lawless

December 1979

Lake Shore Cryotronics, Inc.
64 E. Walnut Street
Westerville, Ohio 43081

I. SUMMARY

Specific heat, thermal conductivity (both in the range 2-30 K), and microhardness data were measured on the ceramics labelled LS-8, LS-8A, and LS-8A doped with CsI, $SnCl_2$, and AgCl. A work-hardened sample of LS-8A was also studied. The goal of this work was to investigate the feasibility of using these types of LS-8 materials to replace Pb spheres in the regenerator of the JPL cryocooler.

The LS-8A materials are all more than an order of magnitude harder than Pb, and the dopants do not significantly improve the hardness. However, the $SnCl_2$ dopant has a remarkable effect in improving the specific heat and thermal conductivity of LS-8A, and this effect was pursued in some detail by measuring samples doped at the 0.1, 0.2, 0.5, 1.0, 1.5, and 2.0% $SnCl_2$ levels. The thermal properties of this series could be described very accurately using analytic models, and the parameters of these models were found to vary smoothly and display extrema with the % $SnCl_2$.

A thermodynamic model was developed to find the optimum $SnCl_2$ doping level. This model incorporated both the specific heat and thermal conductivity parameters and was used to compute the $SnCl_2$ doping level which maximized the regenerator enthalpy change in going from an unloaded to a loaded condition. This optimum doping level in LS-8A is 0.2% $SnCl_2$, which easily enters the LS-8A lattice.

Work-hardening LS-8A appears to have no effect on thermal properties.

Some theoretical comparisons between optimally doped LS-8A and Pb spheres (0.014" diam) are made. For these purposes, the thermal conductance of a packed column of Pb spheres was measured at low temperatures. It is found that the enthalpy change for a regenerator employing the LS-8A material is more than three times larger than for the Pb-spheres case.

Thermal equilibration times for hypothetical spheres of optimally doped LS-8A at low temperatures are estimated. It is found that for sphere sizes below 0.015" diam and for cycle times below 600 rpm the 99% sphere-equilibration times are not exceeded.

Finally, suggestions for the use of rods, rather than spheres, of optimally doped LS-8A in regenerators are discussed.

Table of Contents

II. INTRODUCTION

The effectiveness of regenerators in Stirling-cycle type refrigerators depends critically on matching the specific heat of the regenerator matrix to the specific heat of the working fluid. This effectiveness in turn plays a dominant role in determining the refrigerator efficiency.

In cryogenic refrigerators, or cryocoolers, the working fluid must be He gas, and because He gas retains a large specific heat at low temperatures, the choice of materials for regenerator design is severely limited. Owing to its large volumetric specific heat, Pb is commonly used in cryocooler regenerators; this large specific heat results from the combination of small Debye temperature (108 K) and large density (11.34 gm/cm^3). Since Pb has a rather large thermal conductivity at low temperatures (~1 $W\ cm^{-1}\ K^{-1}$), regenerator designs usually call for Pb spheres in the 0.004-0.020" diam range to minimize the thermal conductance loss across the regenerator.

Two problems plague the use of Pb spheres in cryocooler regenerators: First, bonding between spheres occurs after a relatively small number of cycles, and this increases the axial thermal-conductance loss. Second, and more seriously, at increased cycles the Pb spheres tend to pulverize and thereby degrade the performance and lifetime of the cryocooler.

This proposal was based on a ceramic labelled LS-8 which had the following properties: (1) A volumetric specific heat equivalent to Pb from about 2-30 K; (2) A thermal conductivity smaller than Pb; and (3) A hardness about an order of magnitude larger than Pb.

These properties suggested that the LS-8 ceramic be studied as a possible substitute for Pb spheres to improve the performance and reliability of the JPL cryocoolers. The approach taken was to investigate the effects of doping on the low-temperature thermal properties, and the original purpose of the dopings was to see what improvements in the hardness could be affected by doping, by analogy with the doped alkali halides.[1] Two levels of doping studies were involved: First, a broad view of dopings with CsI, AgCl, and $SnCl_2$; and second, a concentrated study of one or more of these dopants. These dopants were selected based on the ease with which they enter LS-8 which itself is a solid solution.

As will be seen below, the research shifted almost immediately from LS-8 to a neighboring solid solution labelled LS-8A. The reason for this shift was that it was discovered very early on that LS-8A was about 30% harder than LS-8 and was more easily extruded. Therefore, the doping studies mentioned above were applied to LS-8A, and a work-hardened sample of LS-8A was also studied since any spheredization technique would invariably work harden the material.

In parallel with the above doping studies, work was devoted to gaining experience with extruding 0.015" diam rods of pure LS-8A and with slicing

these rods into right circular cylinders 0.015" high. A sample lot of these cylinders (~2 cm^3) was submitted to JPL for initial testing.

In the final stage of the program, an optimum dopant level was decided upon according to a thermodynamic model, and 0.015" diam spheres were fabricated for submission to the JPL.

III. EXPERIMENTAL METHODS

Specific Heat

Specific heat measurements, 2-30 K, were made in the adiabatic pulse calorimeter described previously.[2] Briefly, a 2-3 gm pellet was outfitted with a manganin heater (~300Ω), a carbon chip resistor (~10 mg), and a thermal link (.005" diam manganin wire plus .001" diam Cu wire). A small amount of GE 7031 varnish was used in the assembly, and addenda weights were determined by weighing. The sample was suspended from the thermal link within the adiabatic shield of the calorimeter, and very hard vacuum conditions were maintained throughout the experiment, including the cooldown from room temperature.

A datum consisted of pulsing the sample via the heater with a known current for a measured length of time. The pulse time Δt(~2-10 sec) was always maintained very small in comparison to the time constant of the thermal link so that corrections for the heat flow into the reservoir were negligible. The temperature changes $\Delta T/T$ were maintained in the range 2-4%.

The carbon chip resistor was calibrated in the course of the run against a calibrated Ge resistance thermometer. About a dozen calibration points were taken (2-30 K), and the fitting equation used was[3]

$$\log R = A + BT^{-P} \qquad (1)$$

This equation fitted the R-T data to about ±20 mK.

Owing to the large specific heats of these LS-8 type ceramics, the addenda contributed only about 1% to the total heat capacity, and literature data were used to make the addenda corrections. The method is believed to have an overall uncertainty in the specific heat of ±2% or less.

Thermal Conductivity

Thermal conductivity measurements were made in the same calorimeter. The sample was in the form of a long bar, approximately 3 x 0.6 x 0.2 cm^3, and one end of the bar was thermally anchored to the reservoir by attaching the end to a copper stud with either GE 7031 varnish or silver epoxy. The copper stud bolted into the reservoir. The other end of the bar was fixtured with a manganin heater (~300Ω), and two carbon chip resistors were varnished to the bar about 1 cm apart. The thermometer leads were tempered to the bar, and the measurement consisted of developing a temperature gradient across the bar with the heater and measuring the difference between the two thermometers. The $\Delta T/T$ values were maintained at 2-5%.

The carbon chip resistors were calibrated in the course of the run against the Ge thermometer accord ng to Eq.(1); however, only the B and P coefficients in Eq.(1) were retained from this fitting. The carbon resistors were calibrated at each point against the reservoir temperature, T_o, before applying heat via the sample heater, and the coefficient A in Eq.(1) was determined from this point. That is, A was determined at each reservoir set point, and this procedure obviated the ±20 mK uncertainty in the overall fit according to Eq.(1). In other words, only the coefficients in d log R/dT of Eq.(1) were retained from the overall fit. Note that temperature differences between two calibrations are involved in this measurement, and this procedure is believed to reduce the uncertainty in the temperature measurement to ±5 mK or less.

The largest source of error in the absolute thermal conductivity measurement is the uncertainty in measuring the thermometer separation, ≤5%. On a relative basis, however, the overall uncertainty is ≤1%.

In the course of the program, it became clear that the thermal conductance of a packed column of Pb spheres should be measured, and for this measurement a different method was used. The Pb spheres were packed into a thin-walled plastic straw and both ends plugged with silver epoxy. Two separate heaters were wrapped on the midsection of the straw about 2 cm apart, and a carbon chip resistor thermometer was fixtured to the top of the straw. The bottom of the straw was fixed to the reservoir. In this method, the lower heater is activated and the thermometer measured at steady state. Then, the lower heater is turned off, the upper heater turned on, and the power dissipated in the upper heater is adjusted to exactly match the previous power of the lower heater. At steady state, the thermometer is again measured, and the thermal conductivity is calculated knowing the heater power, the two temperatures, and the separation of the heaters. Here, also, the largest source of error is the uncertainty in measuring the heater separation, ~±5%.

The thermometer calibration for this two-heater method was handled identically to the two-thermometer method.

Microhardness

The microhardness measurements were made on a Scimadzu Type M (#73092) microhardness tester using the standard method of measuring the dimensions of the indent formed by a pyramidal point under a certain load for a specified length of time. In our measurements, a Knoop indenter loaded between 25 and 50 gm for 5 to 30 sec was used. About half a dozen indents were made on each sample and averages taken.

Prior to testing, the samples were polished using first 10 μm, followed by 1 μm, alumina powder slurries. Care was taken to avoid work hardening the material.

IV. EXPERIMENTAL RESULTS

Microhardness

We shall first discuss the microhardness results because these measurements immediately shifted the focus of the program for LS-8 to LS-8A, as noted previously, and because the original purpose of the dopants was to improve the hardness.

The microhardness data for all the materials studied are given in Table I together with the densities. The microhardness of Pb in Table I is taken from the literature.[4]

Table I

Material	Density, gm/cm^3	KHN, Kg/mm^2
Pb	11.344	3.10 ± 0.21
LS-8	6.737	33.7 ± 1.70
LS-8A	7.384	40.5 ± 0.80
LS-8A, work hardened	7.255	45.0 ± 6.05
LS-8A, 0.1% $SnCl_2$	7.481	42.0 ± 1.25
LS-8A, 0.2% $SnCl_2$	7.417	37.2 ± 0.93
LS-8A, 0.5% $SnCl_2$	7.216	37.2 ± 1.93
LS-8A, 0.5% CsI	7.347	47.9 ± 1.03
LS-8A, 0.5% $SnCl_2$ + 0.5% CsI	7.247	40.8 ± 4.44
LS-8A, 1.0% $SnCl_2$	7.092	45.3 ± 3.09
LS-8A, 1.0% $SnCl_2$ + 1.0% CsI	7.221	41.0 ± 1.85
LS-8A, 1.5% $SnCl_2$	7.217	-
LS-8A, 2.0% $SnCl_2$	7.081	-

Table I immediately shows two main features: First, all of the LS-8 type ceramics are at least an order of magnitude harder than Pb; and second, LS-8A has both a larger hardness and a larger density than LS-8. This latter point is important because specific heat on a volumetric basis is needed for regenerator applications. Also, as will be seen below, LS-8A has a larger specific heat than LS-8 above 7 K. Therefore, the program re-direction to LS-8A made excellent sense.

The first round of studies involved the following LS-8A samples: Work-hardened, 0.5% CsI, 0.2% $SnCl_2$, and 0.5% AgCl. As seen in Table I, work-hardening increases the hardness, as expected (40.5 to 45.0), and CsI appears to be an attractive hardening dopant (40.5 to 47.9).

As will be seen below, the $SnCl_2$ dopant leads to improved low temperature thermal properties, so the second round of doping studies

concentrated on the CsI and $SnCl_2$ dopants. Specifically, 0.1, 0.5, 1.0, 1.5, and 2.0% $SnCl_2$, and the mixed dopants, 0.5 and 1.0% each of $SnCl_2$ and CsI. The goal here was to explore further the thermal properties improvement with $SnCl_2$ doping and to see if the mixed dopants would lead to improvements in both thermal and hardness properties.

This, however, was not found in the case of the additional CsI dopings, as seen in Table I. Although CsI by itself is an effective hardner, in combination with $SnCl_2$ there is no effect on the hardness.

The sequence of $SnCl_2$ dopings shows a decrease in hardness between 0.2 and 0.5% (40.5 to 37.2). The 1.5 and 2.0% samples were not measured for reasons to be discussed below.

The microhardness measurement also provides qualitative information on the homogeneity and uniformity of the sample. In the case of the 1.0, 1.5, and 2.0% $SnCl_2$ samples, there was evidence of the formation of a second phase. The $SnCl_2$ dopings at and below 0.5% showed excellent homogeneity.

Specific Heat

Specific heat measurements were made on all samples in the program, and Figs. 1-3 show the specific heat data measured on the first round of samples. These data are plotted as C/T^3 vs. T, where C is the volumetric specific heat, and the temperatures are plotted on a T^2 scale. There are several reasons for plotting the data in this fashion. Primarily, both C and T^3 change by several orders of magnitude from 2-30 K, so comparisons between materials are easier to visualize on a C/T^3 plot. In addition, the maxima in C/T^3 indicate the presence of an Einstein mode added to the Debye (i.e., C/T^3 = constant) background, and we will make use of this later in the data analysis. Finally, we note that a C/T^3 plot is the most demanding way to plot experimental data.

The data for Pb in these plots was estimated using literature data[5] (Θ_D = 108 K, γ = 0.0036 J mole^{-1} K^{-2}) for pure bulk Pb.

Figure 1 compares LS-8 and LS-8A to Pb. Both LS-8 and LS-8A have larger volumetric specific heats than Pb between 3-20 K, but the LS-8A specific heat is larger than that of LS-8 between 7-30 K. As noted above, this was additional evidence for re-directing the program to LS-8A.

Figure 2 shows the specific heats of pure, 0.5% CsI doped, and 0.5% AgCl doped LS-8A compared to Pb. The CsI doping, while useful as a hardener, has virtually no effect on the specific heat of LS-8A. The AgCl doping increases the specific heat of LS-8A below 12 K, but this was not pursued with further AgCl dopings because of the discovery of the $SnCl_2$ doping effects discussed below.

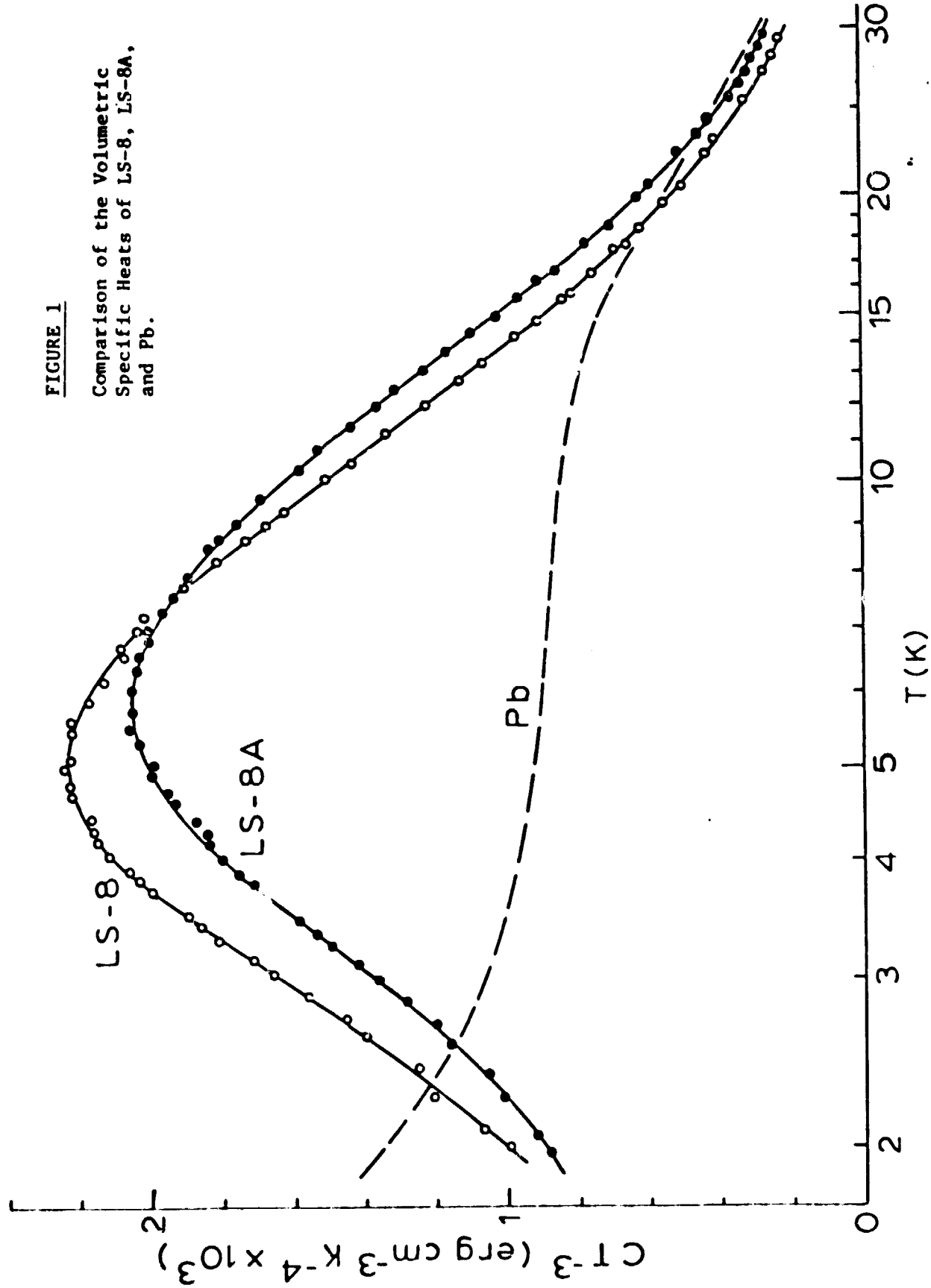

FIGURE 1

Comparison of the Volumetric Specific Heats of LS-8, LS-8A, and Pb.

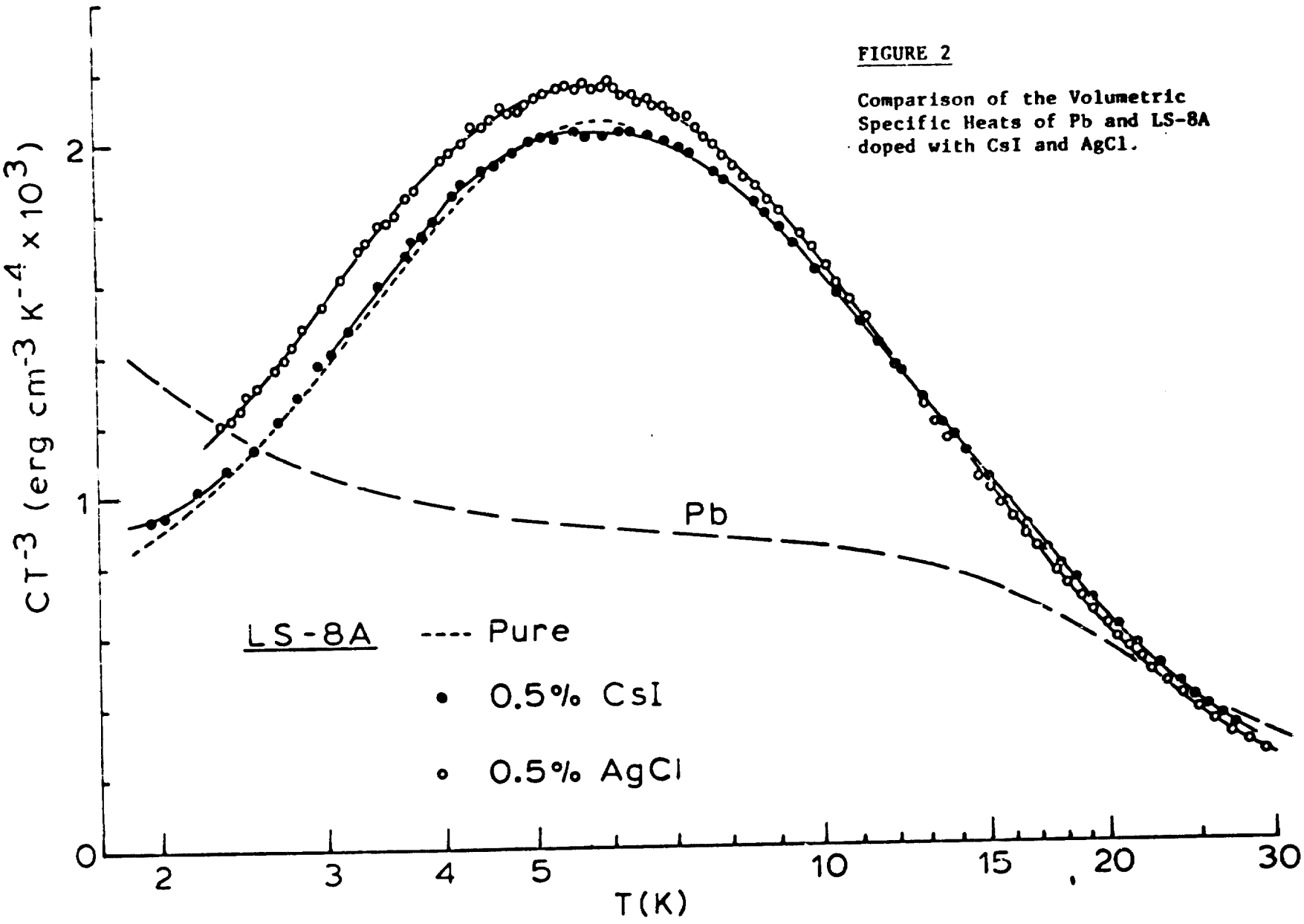

FIGURE 2

Comparison of the Volumetric Specific Heats of Pb and LS-8A doped with CsI and AgCl.

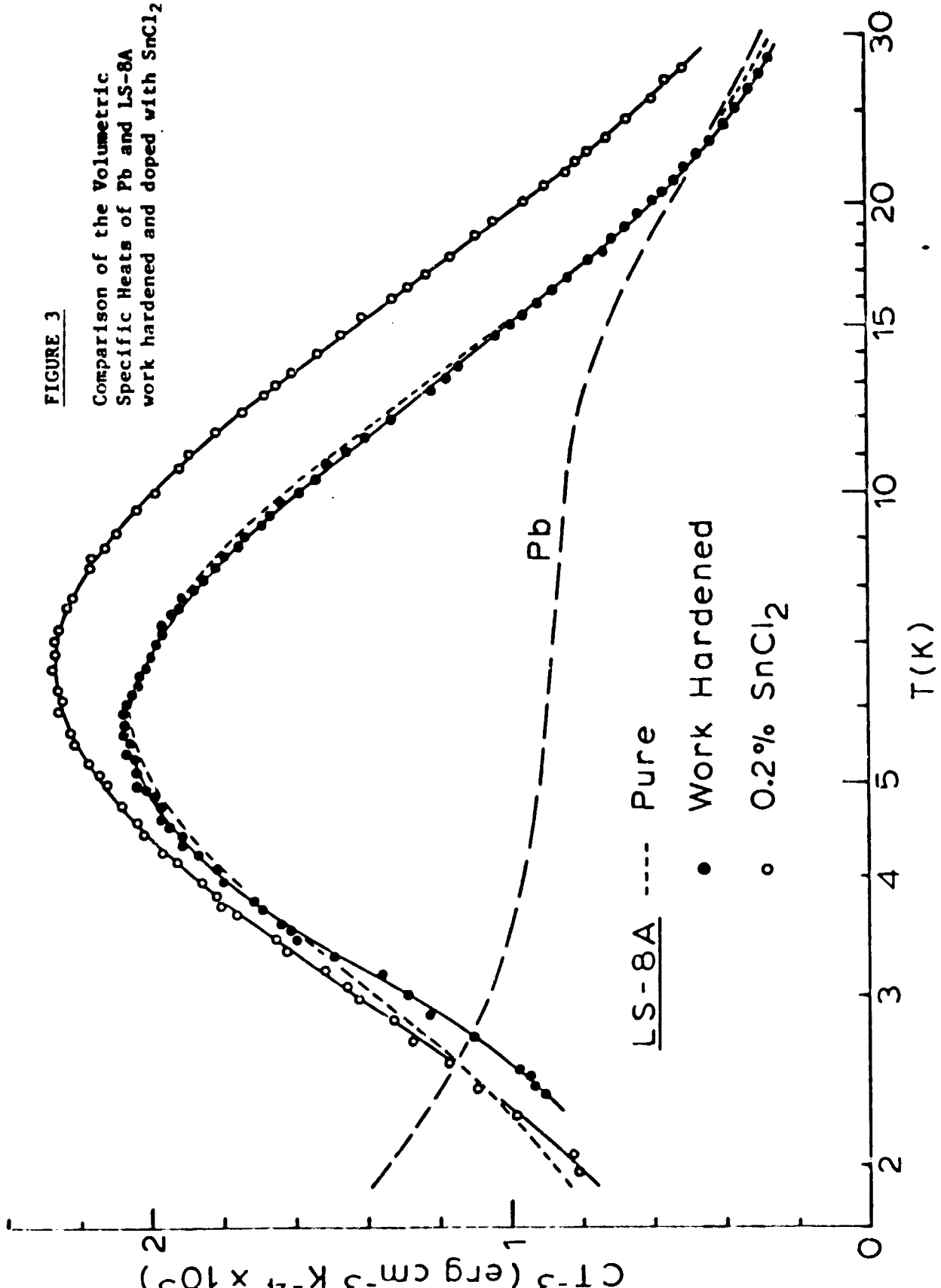

FIGURE 3

Comparison of the Volumetric Specific Heats of Pb and LS-8A work hardened and doped with $SnCl_2$.

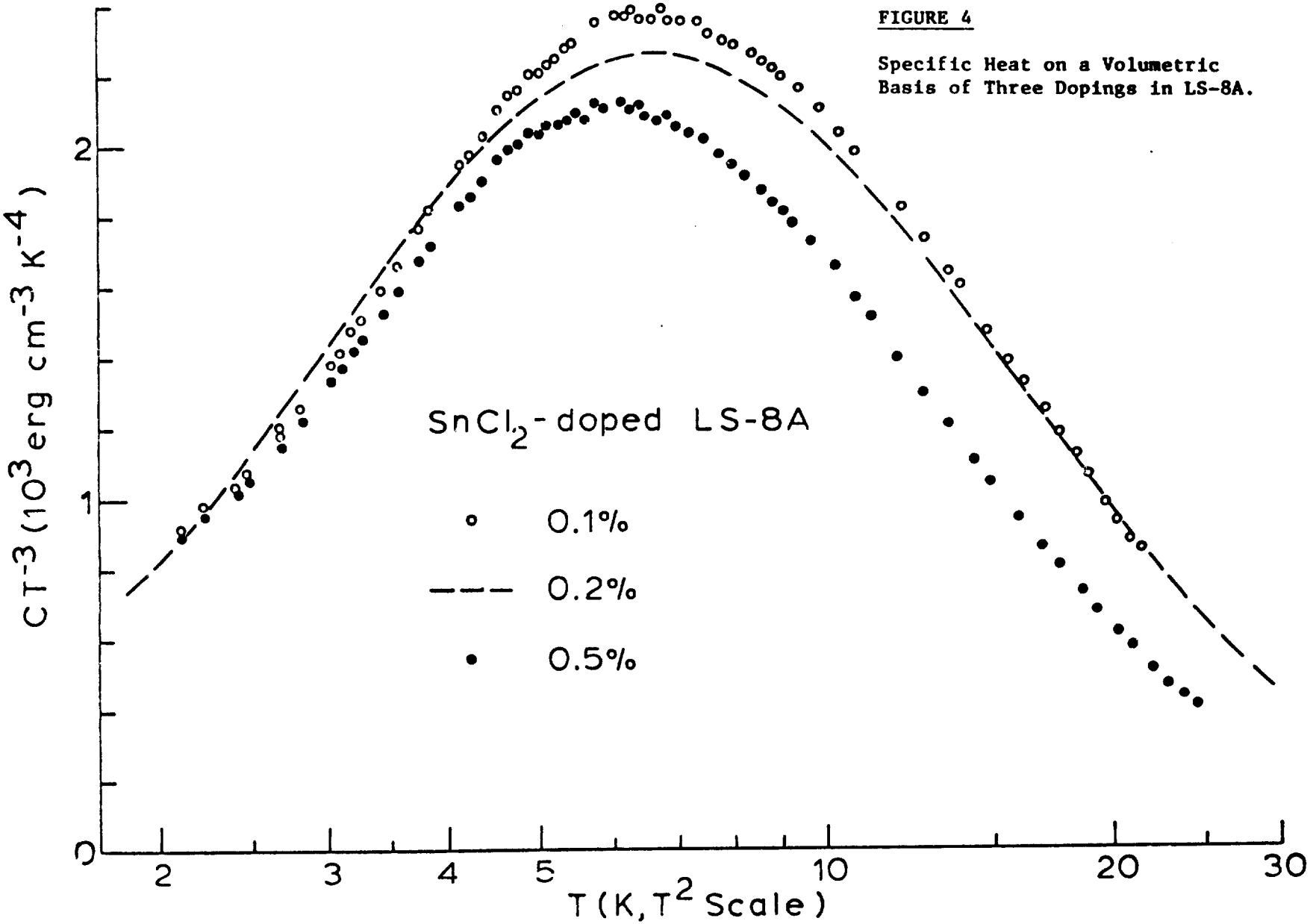

FIGURE 4

Specific Heat on a Volumetric Basis of Three Dopings in LS-8A.

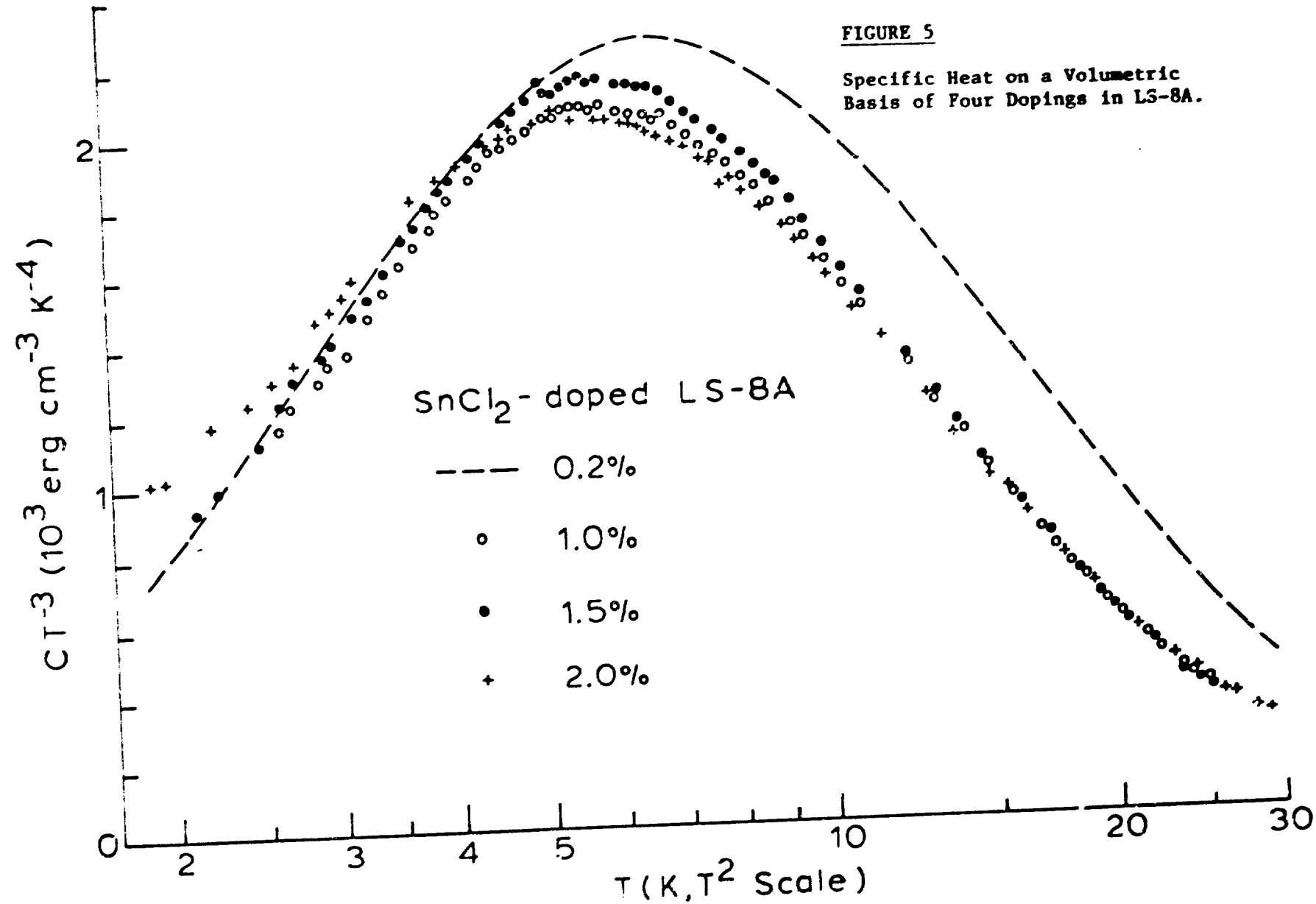

FIGURE 5

Specific Heat on a Volumetric Basis of Four Dopings in LS-8A.

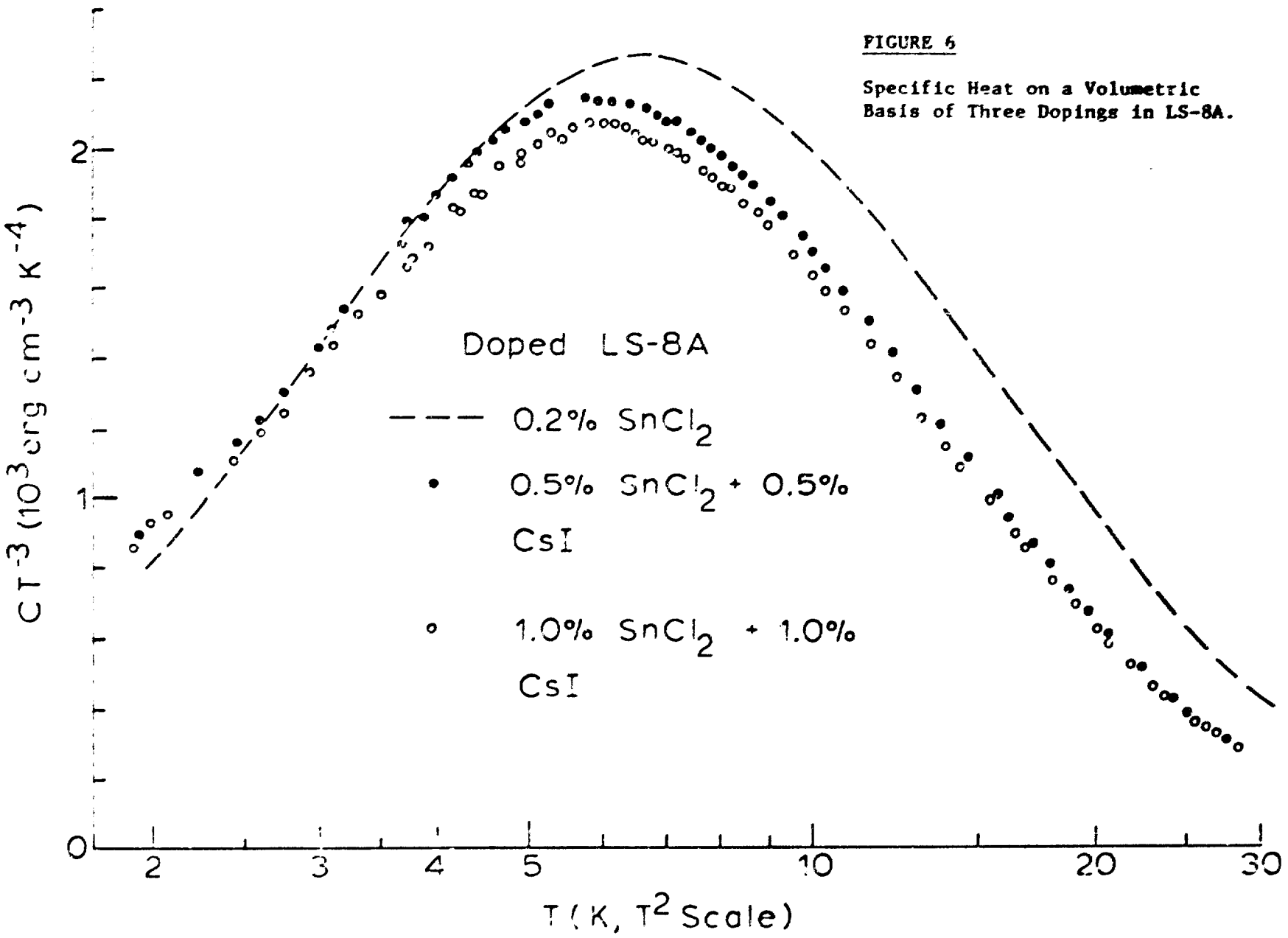

FIGURE 6

Specific Heat on a Volumetric Basis of Three Dopings in LS-8A.

Figure 3 shows the specific heats of pure, work-hardened, and 0.2% $SnCl_2$ doped LS-8A compared to Pb. This figure shows two remarkable features: First, the 0.2% $SnCl_2$ doping leads to a very large increase in the specific heat of LS-8A; and second, work hardening does not appreciably effect the specific heat of LS-8A.

The remarkable effect of the $SnCl_2$ doping on the LS-8A specific heat made this an irresistable dopant to pursue further. Note in particular from Fig. 3 that the $SnCl_2$ doped sample has a larger specific heat than Pb at 30 K.

The next sequence of $SnCl_2$-doped LS-8A samples had levels of 0.1, 0.5, 1.0, 1.5, and 2.0%, in addition to the mixed $SnCl_2$ + CsI dopings for hardness purposes, as discussed above. Specific heat data on these samples are shown in Figs. 4-6.

Figure 4 shows the specific heats of the 0.1, 0.2, and 0.5% $SnCl_2$ doping levels in LS-8A. The significant feature in Fig. 4 is that the specific heat of LS-8A appears optimized by doping levels in the 0.1-0.2% range, and the 0.1% level actually yields the larger specific heat. The 0.5% level leads to a specific heat not much different from pure LS-8A (compare with Fig. 3).

Figure 5 shows the effect of $SnCl_2$ doping levels between 1-2% on the specific heat, and the specific heat of all of these samples is not much different from pure LS-8A and unmistakenly smaller than that of the 0.2% $SnCl_2$-doped sample.

Figure 6 shows the specific heat data for the mixed $SnCl_2$ + CsI dopings, and here also these specific heats are not much different from that of pure LS-8A.

Thermal Conductivity

Thermal conductivity data measured on the first round of samples are shown in Fig. 7. These data reveal that the AgCl and $SnCl_2$ dopings markedly improve the thermal conductivity of LS-8A below about 10 K, whereas the CsI doping considerably "flattens" the thermal conductivity. Work hardening does not appreciably affect the thermal conductivity of LS-8A (curve labelled W. H. in Fig. 7). The thermal conductivity of LS-8A above about 20 K is independent of the doping and approaches about 10 mW cm^{-1} K^{-1}.

The effect of various $SnCl_2$ doping levels on the thermal conductivity of LS-8A is shown in Fig. 8 for doping levels up to 1.0%. Here an interesting effect is seen, in that the thermal conductivity curve is most fully developed for the 0.2% doping level. The doping levels above and below this value lead to depressed thermal conductivity curves, including the case of pure LS-8A.

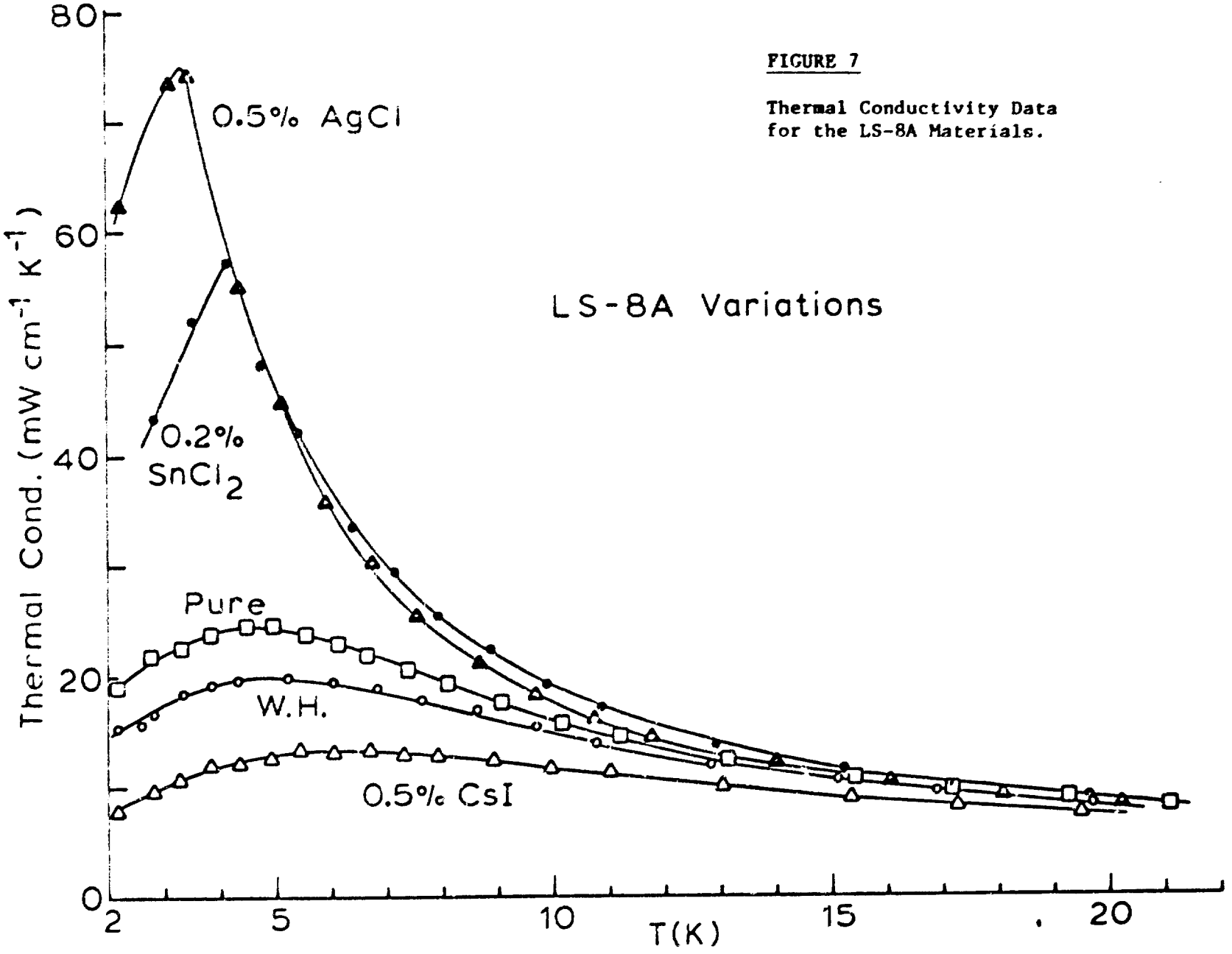

FIGURE 7

Thermal Conductivity Data for the LS-8A Materials.

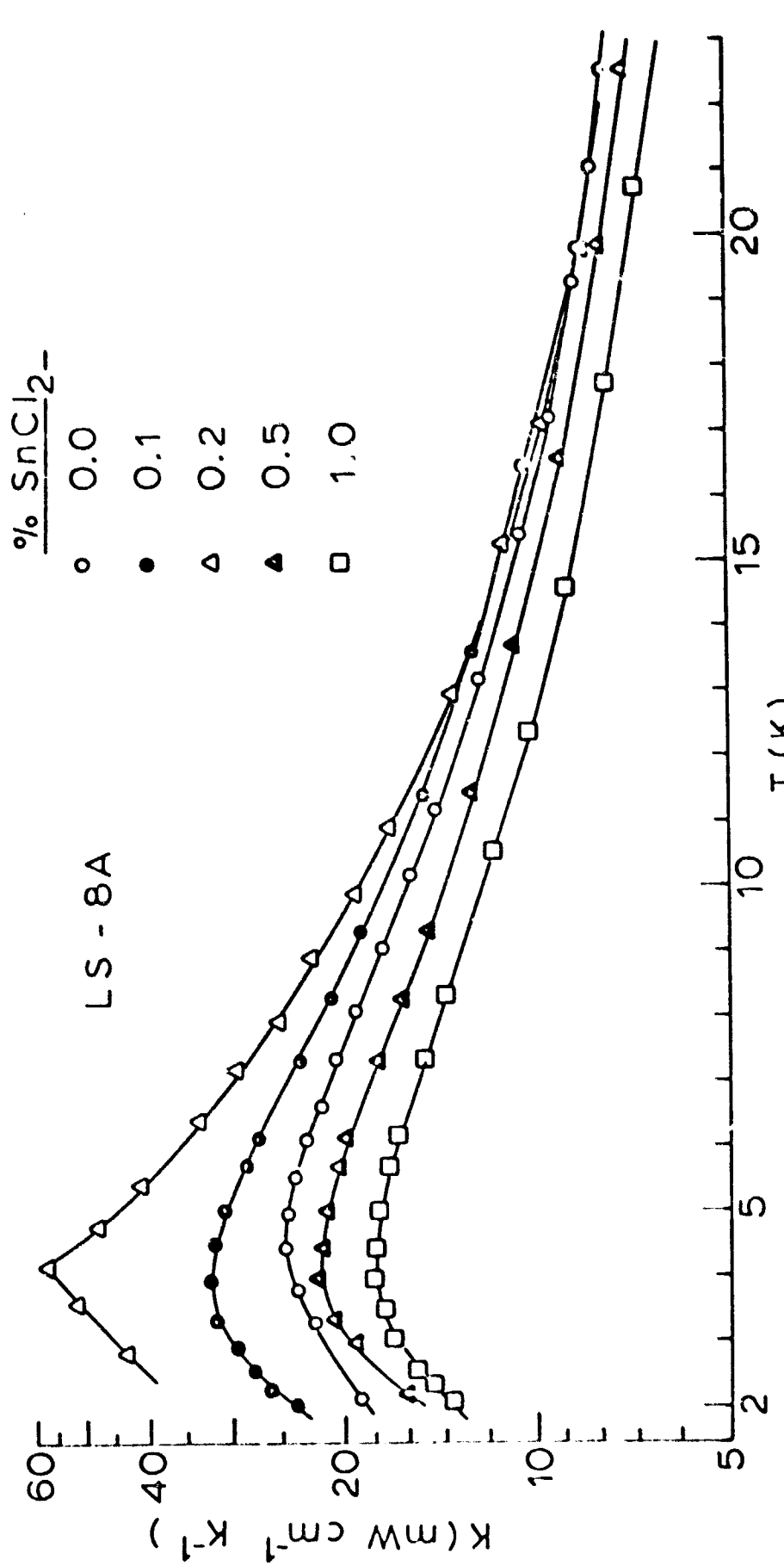

FIGURE 8 Thermal Conductivity Data on the Sequence of $SnCl_2$-doped LS-8A Samples.

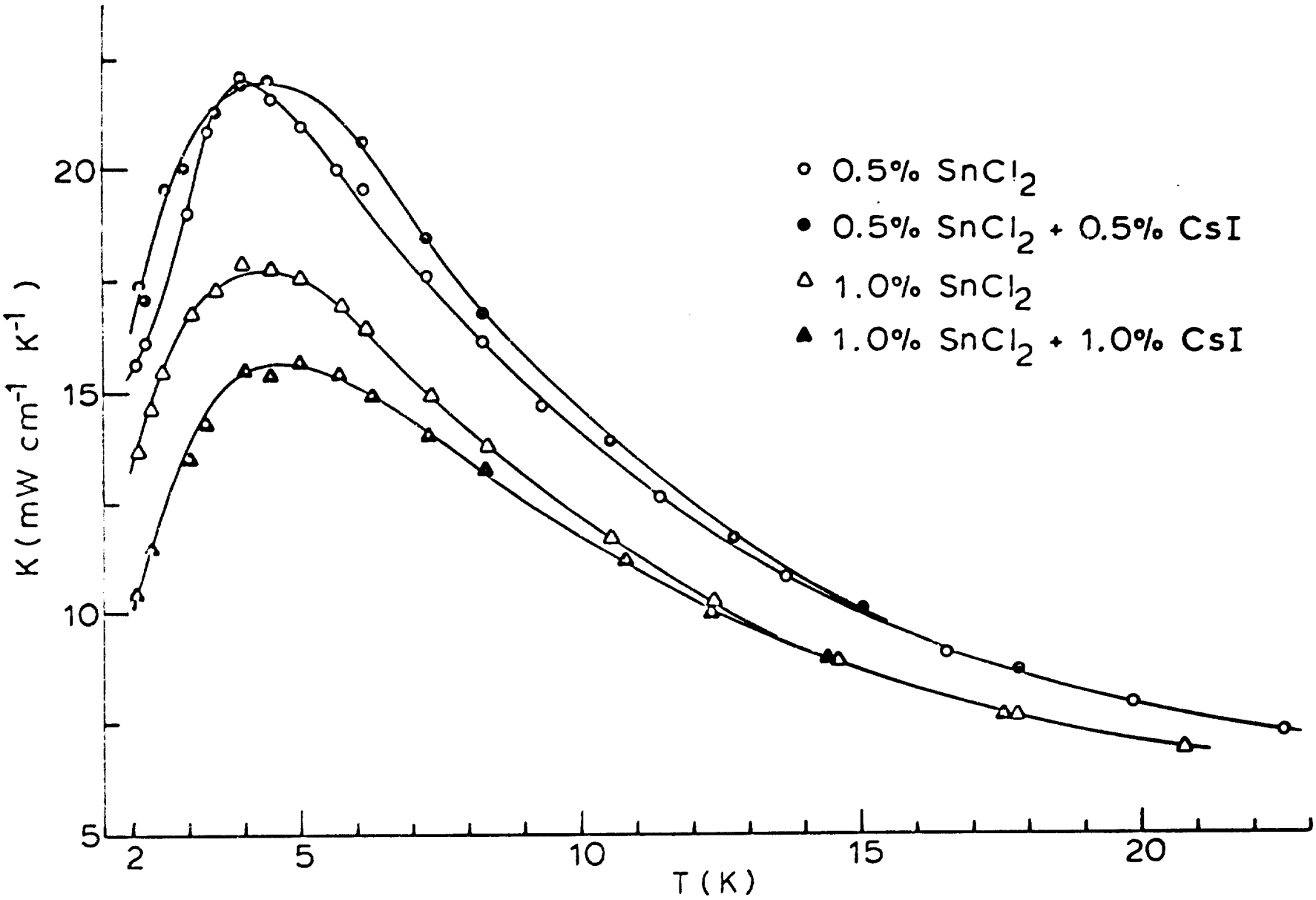

FIGURE 9 Thermal Conductivity Data on the Mixed $SnCl_2$ + CsI-doped LS-8A Samples.

Finally, in Fig. 9, are shown thermal conductivity data for the mixed CsI + $SnCl_2$ dopings compared to the $SnCl_2$ dopings alone. It is apparent from Fig. 9 that augmenting the $SnCl_2$ doping with a CsI doping at the same level has very little effect on the thermal conductivity.

V. DISCUSSION OF RESULTS

Doping Effects

The above section presents a great deal of experimental data on the effects on the microhardness and low-temperature thermal properties of LS-8A resulting from dopings with AgCl, $SnCl_2$, and CsI, which are the most favorable dopants for entering the LS-8A lattice.

Also presented are data comparing LS-8 and LS-8A, and it is now seen that LS-8A is the more favorable basic material from the standpoint of microhardness (Table I) and volumetric specific heat (Fig. 1).

In addition, it was observed in the microhardness measurements that LS-8 is more brittle than LS-8A because the pyramidal identer made an indent that was somewhat shattered, in contrast to the well-defined indents observed in LS-8A.

Although a great deal of effort was expended on studying the CsI dopant because of the initial microhardness result (Table I), this dopant turned out to be somewhat of a blind alley. In combination with the $SnCl_2$ dopant, the CsI dopant did not lead to improved microhardness (Table I), as originally expected. The CsI dopant appears completely passive in its effect on the thermal properties of LS-8A when used in conjunction with the $SnCl_2$ dopant (Figs. 6 and 9). Along this line, it is interesting to observe that the 0.5% CsI doping alone flattens the thermal conductivity (Fig. 7) whereas the 0.5% CsI + 0.5% $SnCl_2$ dopings result in a maximum in the thermal conductivity (Fig. 9).

The outstanding discovery in these doping studies is the improvement in specific heat and thermal conductivity resulting from the $SnCl_2$ dopant. There is ample evidence that the $SnCl_2$ doping (at small levels) leads to a greater degree of crystal perfection in LS-8A: For example, at 0.2%, the thermal conductivity (Fig. 5) approaches the perfect crystal behavior showing the onset of boundary scattering. There is also clear evidence that this crystalline perfection tends to degenerate at doping levels above 0.2%: Namely, the thermal conductivity curves at 0.5 and 1.0% (Fig. 5) are depressed and flattened, and this broadening and flattening are indicative of phonon scattering from microcrystalline imperfections. The microhardness data correlate well with these observations because evidence of the formation of a second phase in LS-8A was seen at $SnCl_2$ doping levels of 1% and higher.

Einstein Modes in LS-8A

The C/T^3 data in Figs. 1-6 all show maxima around 2.5 K ($T^2 \sim 7$), and this behavior indicates a strong contribution from an Einstein mode (or modes) due probably to an acoustic phonon. This can be understood by considering the simple model of an Einstein term added to the Debye term,

namely

$$C = C_D(\Theta_D/T) + 3Rry^2e^y/(e^y-1)^2,\ y = \Theta_E/kT \qquad (2)$$

where C_D, Θ_D are the Debye function and temperature, r is the density of Einstein oscillators per formula weight, and $\Theta_E = h\nu_E/k$ is the Einstein temperature, ν_E being the Einstein oscillator frequency. Now, C_D has the property that at low temperatures C_D/T^3 = constant, so that a maximum in C/T^3 comes from the Einstein term. Equation (2) has the property that C/T^3 has a maximum at a temperature $T_{max} = \nu_E/3$.

In the most general case, Eq. (2) would contain a sum over several Einstein terms, but it has been found here that a single Einstein term yields an excellent fit to all the specific heat data measured on the LS-8A materials. A three-level (i.e., Θ_D, Θ_E, and A = r/2), non-linear regression-analysis computer program was used to analyze these specific heat data, and in Figs. 10-12 are shown examples of the data fits obtained with Eq. (2). These data involve the excess specific heat $C_{ex} = C-C_D$ and are plotted vs 1/T which is the low temperature form of Eq. (2) (i.e., $T<<\Theta_E$). The curvature in the plots is due to plotting according to this form.

As seen in Figs. 10-12, excellent fits to the experimental data were obtained over several orders of magnitude in $T^2C_{ex}/3R$. The correlation cofficients in these fits were typically ≥99%. The parameters resulting from these fits for the $SnCl_2$-doped LS-8A ceramics are summarized in Table II (although all specific heat data were fitted, only the $SnCl_2$ doping results are of interest here).

Table II (LS-8A)

Dopant	Θ_D	Θ_E	A
Pure LS-8A	99.40	27.69	0.0976
0.1% $SnCl_2$	95.62	33.19	0.2069
0.2% $SnCl_2$	93.99	32.71	0.1816
0.5% $SnCl_2$	100.50	27.96	0.1110
0.5% $SnCl_2$ + 0.5% CsI	98.77	27.36	0.1039
1.0% $SnCl_2$	100.81	26.78	0.0984
1.0% $SnCl_2$ + 1.0% CsI	99.77	27.47	0.0985

The Table II data show the remarkable property that Θ_D, Θ_E, and A(= r/2) have extremal values as a function of $SnCl_2$ doping; Θ_D at 0.2% Θ_E and A at 0.1%.

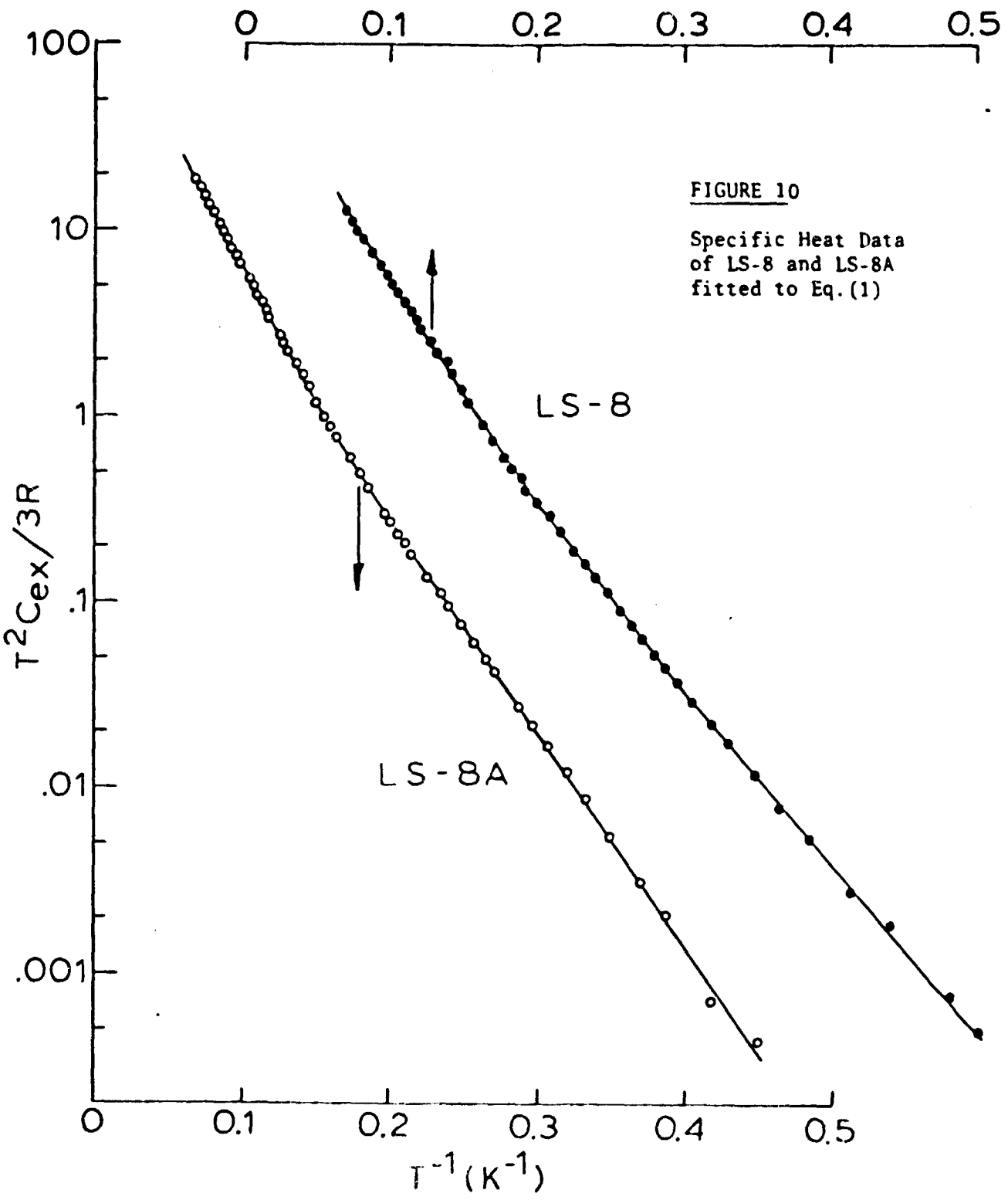

FIGURE 10

Specific Heat Data of LS-8 and LS-8A fitted to Eq. (1)

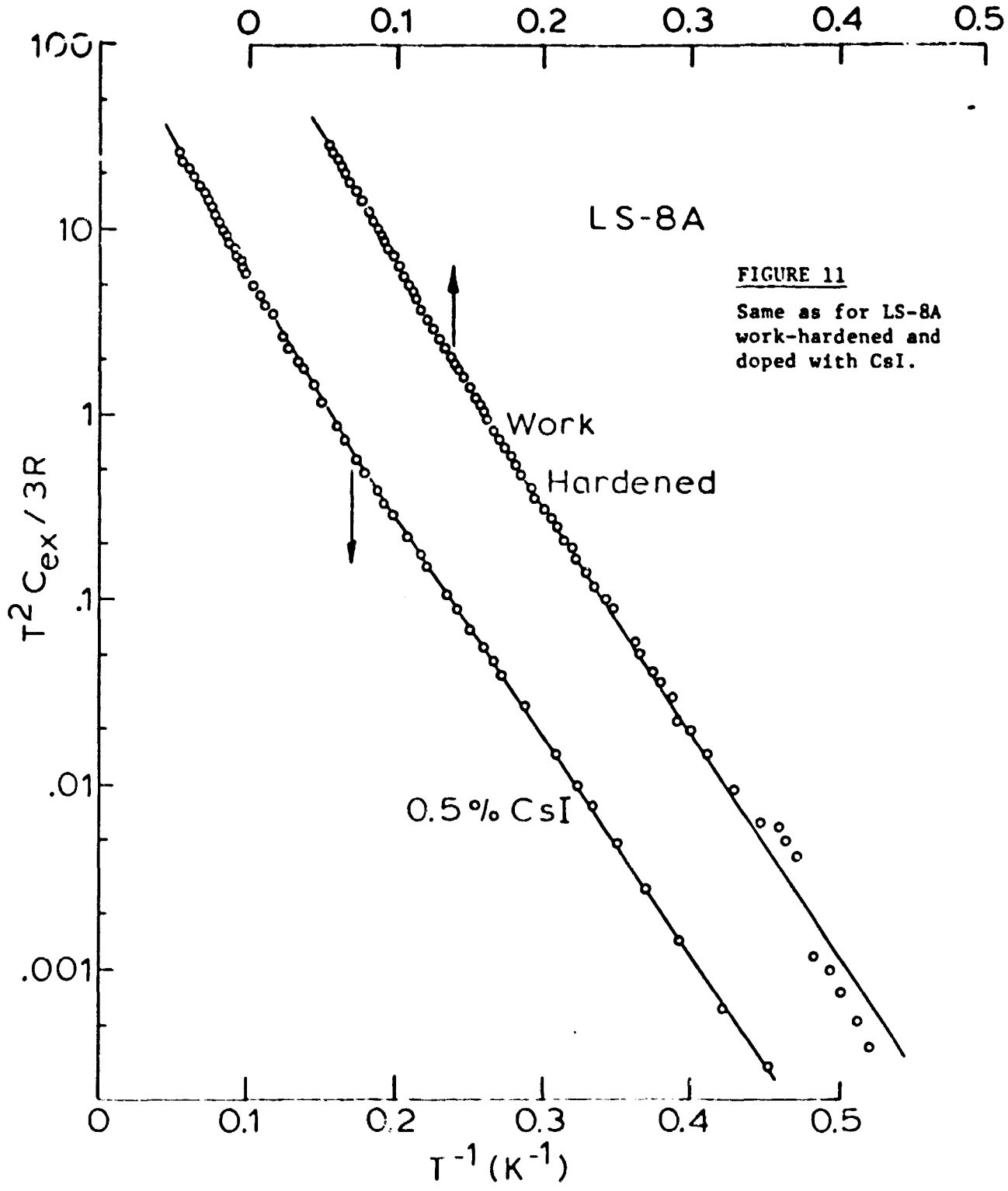

FIGURE 11

Same as for LS-8A work-hardened and doped with CsI.

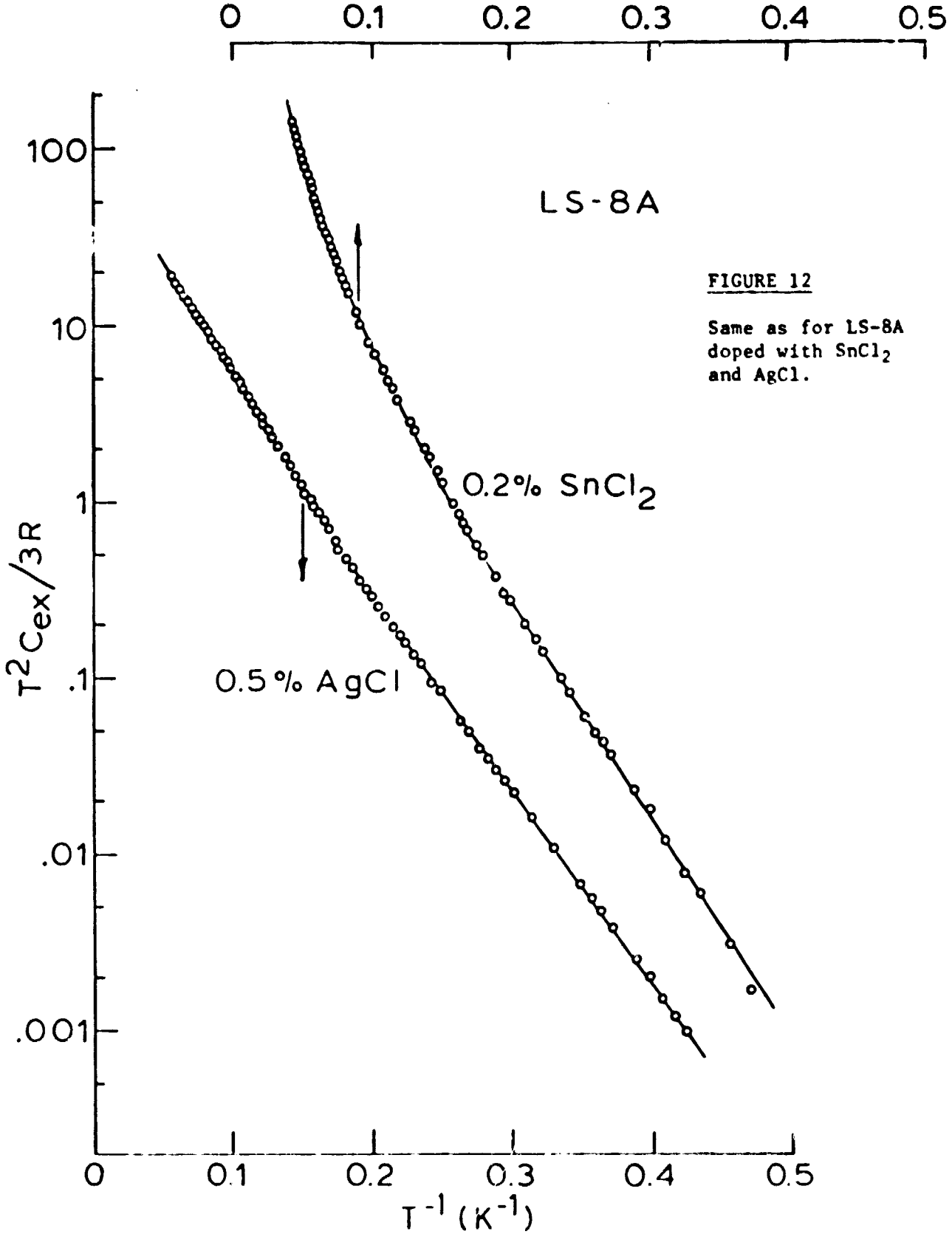

FIGURE 12

Same as for LS-8A doped with $SnCl_2$ and AgCl.

Thermal Conductivity

As seen in Figs. 7-9, the thermal conductivity of the LS-8A materials decreases with increasing temperature. It was found that this behavior could be accurately described by the simple power law,

$$K = BT^m, \tag{3}$$

and in Fig. 13 are shown the thermal conductivity data for the $SnCl_2$-doped LS-8A materials above 5 K. In all cases, the data are described very accurately by Eq. (3), and fitted values for the coefficients m are given in Fig. 13. Here again, we note that m has an extremal value with the % $SnCl_2$ doping level.

Thermodynamic Model

In the above we have parameterized our experimental data on $SnCl_2$-doped LS-8A according to a specific heat model, Eq. (2), and a phenomenological thermal conductivity relation, Eq. (3). All of these parameters, and also the density (Table I), display extremal values with the % $SnCl_2$ doping, and all of these data are shown plotted in Fig. 14 as a function of the % $SnCl_2$, x.

The data in Fig. 14 show some remarkable features, not the least of which is that this large amount of experimental data can be parameterized so smoothly. First, the triangles at the origin (x = 0) refer to the work-hardened LS-8A, and it is seen that work hardening has only a minor effect on the thermal properties. Second, the parameters do not change appreciably between 0.5 and 1.0% $SnCl_2$, which further supports the observation made above that $SnCl_2$ doping levels above 0.5% promote the formation of a second phase. The parameters for the mixed $SnCl_2$ + CsI dopings at 0.5 and 1.0% are also shown in Fig. 14, and here also it is seen that the CsI dopant plays a passive role on the thermal properties.

The parametric data in Fig. 14 now allow us to develop a thermodynamic model for deciding on an optimum $SnCl_2$ doping level.

To begin, we first note that the temperature distribution across a regenerator filled with an LS-8A type material is given by

$$T^{m+1} = T_c^{m+1} + (x/L)(T_H^{m+1} - T_c^{m+1}) \tag{4}$$

where x/L is the normalized axial distance along the regenerator, T_c is the cold-end temperature at x = 0, T_H is the hot-end temperature at x = L, and m is the exponent in Eq. (3). Equation (4) results directly from integrating the linear heat-flow relation using Eq. (3). The effects of the counterflowing He gas in the regenerator are of necessity ignored in Eq. (4).

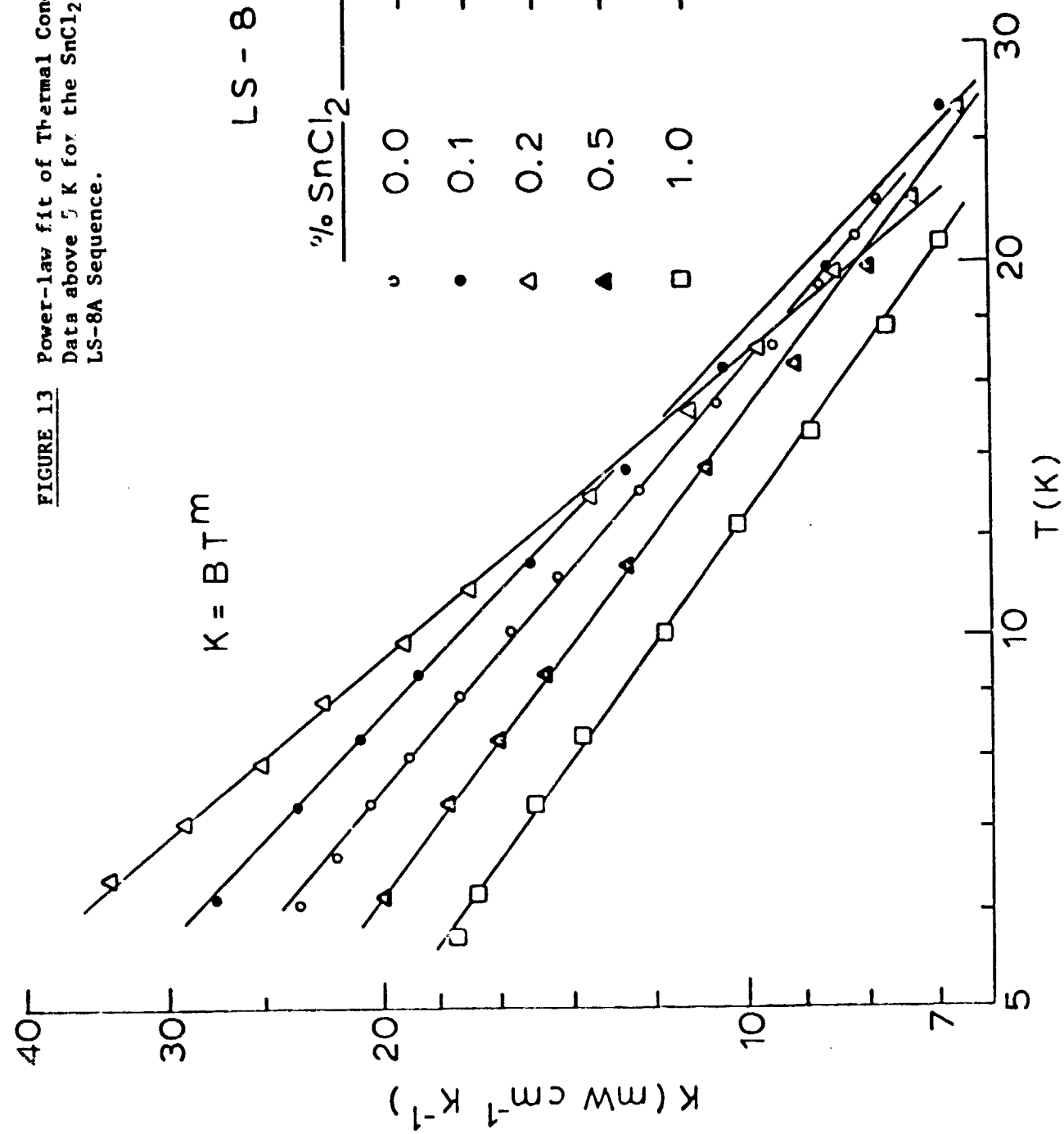

FIGURE 13 Power-law fit of Thermal Conductivity Data above 5 K for the $SnCl_2$-doped LS-8A Sequence.

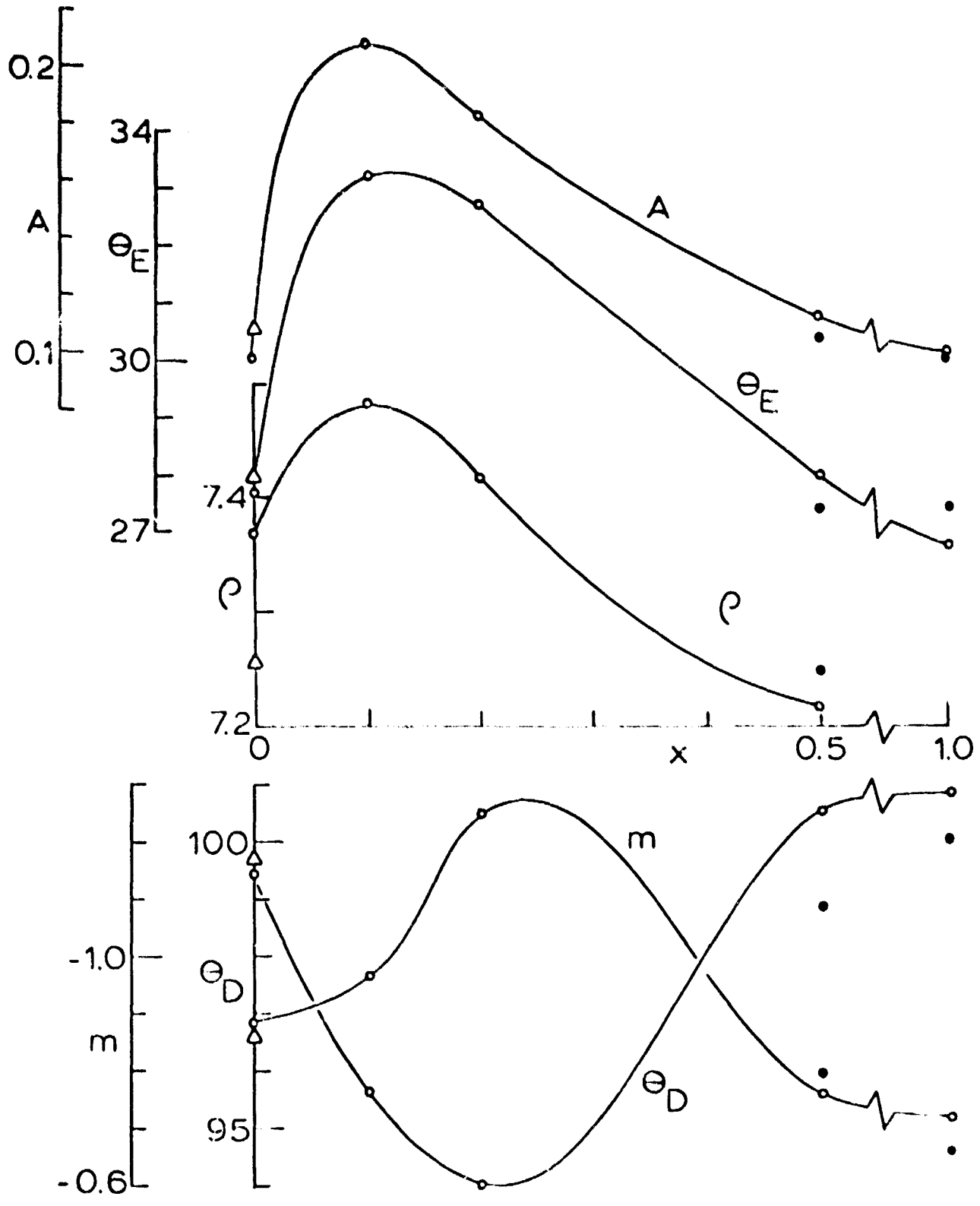

FIGURE 14 Variation in the Density and Thermal-properties Parameters of LS-8A with %$SnCl_2$. The triangles at the origin refer to work-hardened LS-8A, and the solid circles at x = 0.5, 1.0 refer to the $SnCl_2$ + CsI double dopings.

Given the exponent m, Eq. (4) allows direct calculation of the different temperature gradients across a regenerator for a loaded and an unloaded case. A typical hot-end temperature for a regenerator in the second stage of a cryocooler is T_H = 30 K, and this T_H is not much changed between the loaded and unloaded cases, provided the load is not too large. A typical unloaded cold-end temperature is T_{c1} = 8 K, and a typical loaded T_{c2} = 10 K is assumed. Equation (4) then allows calculation of T_1 and T_2 at several x/L positions along the regenerator corresponding to the unloaded and loaded cases.

Next, the enthalpy change at x/L is calculated by integrating the specific heat, Eq. (2), between T_1 and T_2. For this calculation, the specific heat is multiplied by the density ρ to place the enthalpy changes on a volumetric basis. And finally, the total enthalpy change of the regenerator is found by integrating the enthalpy changes at x/L across the regenerator length (x/L = 0 to 1.0).

This procedure can be represented functionally as

$$\Delta H(T_{c1}, T_{c2}, T_H) = \rho \int_0^1 \int_{T_1(m,x/L)}^{T_2(m,x/L)} C(\theta_D, \theta_E, A, T)\, dT\, d(x/L), \qquad (5)$$

and physically the total enthalpy change represents the amount of heat energy that has to be re-distributed within the regenerator in going from the unloaded to the loaded case.

The procedure here is straightforward: For a particular $SnCl_2$ doping level, x in Fig. 14, the corresponding parameter values are selected from the smooth curves of Fig. 14, and Eq. (5) is solved. The numerical integrations in Eq. (5) were solved on a computer, and a second loaded cold-end temperature was also studied, T_{c2} = 12 K.

The results of these computations are shown in Fig. 15 where the enthalpy changes are plotted relative to the maximum enthalpy change. The remarkable results in Fig. 15 show that the results for T_{c2} = 10 and 12 K are practically identical and that the regenerator enthalpy is maximized for a $SnCl_2$-doping level slightly below 0.2%. In addition, the material is very "forgiving" in the sense that the 95% level in Fig. 15 corresponds to x-values of 0.10 to 0.28% on either side of the maximum. These results are very fortunate because, as we have seen, doping levels around 0.2% lead to the best crystalline perfection. Finally, we note from Fig. 4 that the 0.1% level actually leads to a higher specific heat, yet the 0.2% level from Fig. 15 yields the optimum trade-off between specific heat and thermal conductivity exponent.

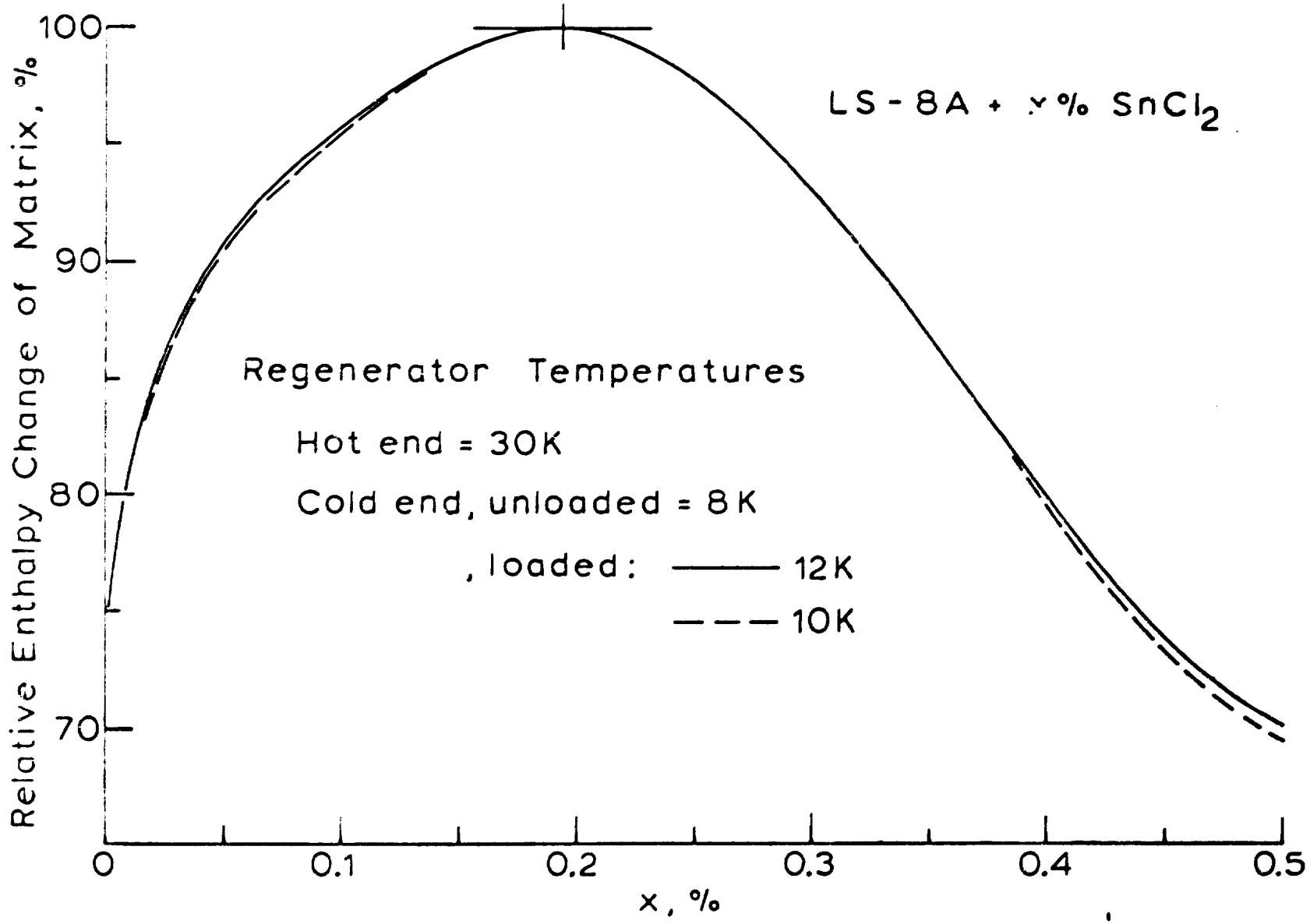

FIGURE 15 Regenerator Enthalpy Changes as a Function of $\%SnCl_2$ in LS-8A.

Comparisons with Pb

We have now developed the necessary data on the optimally $SnCl_2$-doped LS-8A to make some direct theoretical comparisons with Pb spheres. All that is needed for this comparison is the thermal conductivity of a packed column of Pb spheres. These data were measured on plastic straws filled with 0.004" and 0.014" diam Pb spheres by the method mentioned previously (i.e., the two-heater, one-thermometer technique). The packing fraction in the straws was 57%.

The results of these measurements are shown in Fig. 16, and it is interesting to note that the larger spheres show the drop in the thermal conductivity at the superconducting transition temperature. These data approximately follow Eq. (3) above 8 K, and the fitted exponent value for the larger, 0.014" diam spheres is

$$m = 0.533 \text{ (Pb spheres, 0.014" diam)} \qquad (6)$$

The temperature distributions across a regenerator filled with the larger Pb spheres and filled with a hypothetical, 0.2%-$SnCl_2$-doped LS-8A material are shown in the upper plot of Fig. 17 plotted according to Eq. (4). It is assumed here that whatever form the LS-8A material is in (e.g., spheres), the exponent m would be unaffected. There is some evidence supporting this assumption, namely from Fig. 14 work-hardening does not materially affect m. There is of course the effect of increased boundary scattering on ≈0.015" diameter LS-8A spheres, for example (the LS-8A thermal conductivity samples were ≈0.06" thick), and the effect of the intra-sphere thermal resistance. Lacking information on these effects, however, we will assume that the bulk coefficient m can be used.

The dominant difference between the curves in the upper plot of Fig. 17 is that the Pb-spheres plots are concave down, the LS-8A plots, concave upward. The distributions are drawn for an unloaded T_{c1} = 8 K, a loaded T_{c2} = 10 K, and it can be seen that the concave upward curve leads to the best case for maximizing the enthalpy change. The reason for this is simply that the temperature differences T_2-T_1 are still large at large x/L-values, and it is at these higher temperatures that the specific heat, and hence the enthalpy changes, are large.

This effect is illustrated in the lower plot of Fig. 17 where the enthalpy changes across the regenerator are calculated from the curves in the upper plot of Fig. 17 using the literature data[5] for Pb and the experimental data for 0.2%-$SnCl_2$-doped LS-8A, Fig. 3.

The lower plot of Fig. 17 dramatically shows the effect of the negative m-exponent for LS-8A compared to the positive m-exponent for Pb (of course, the 0.2% $SnCl_2$ specific heat is considerably larger than that of Pb, also). The maximum enthalpy change for the LS-8A material occurs at x/L = 0.65 corresponding to T_1 = 19.45, T_2 = 20.84 K. For the

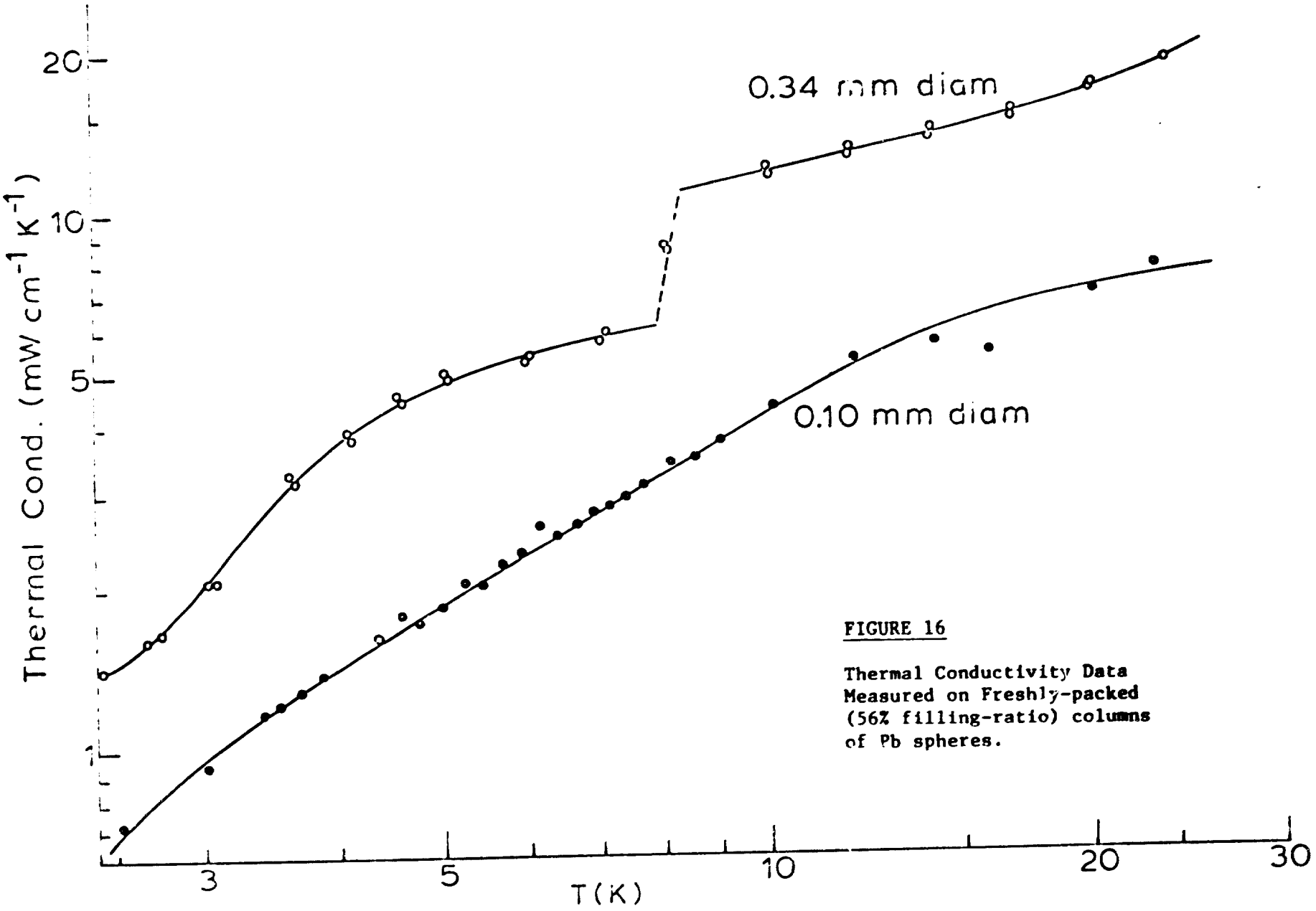

FIGURE 16

Thermal Conductivity Data Measured on Freshly-packed (56% filling-ratio) columns of Pb spheres.

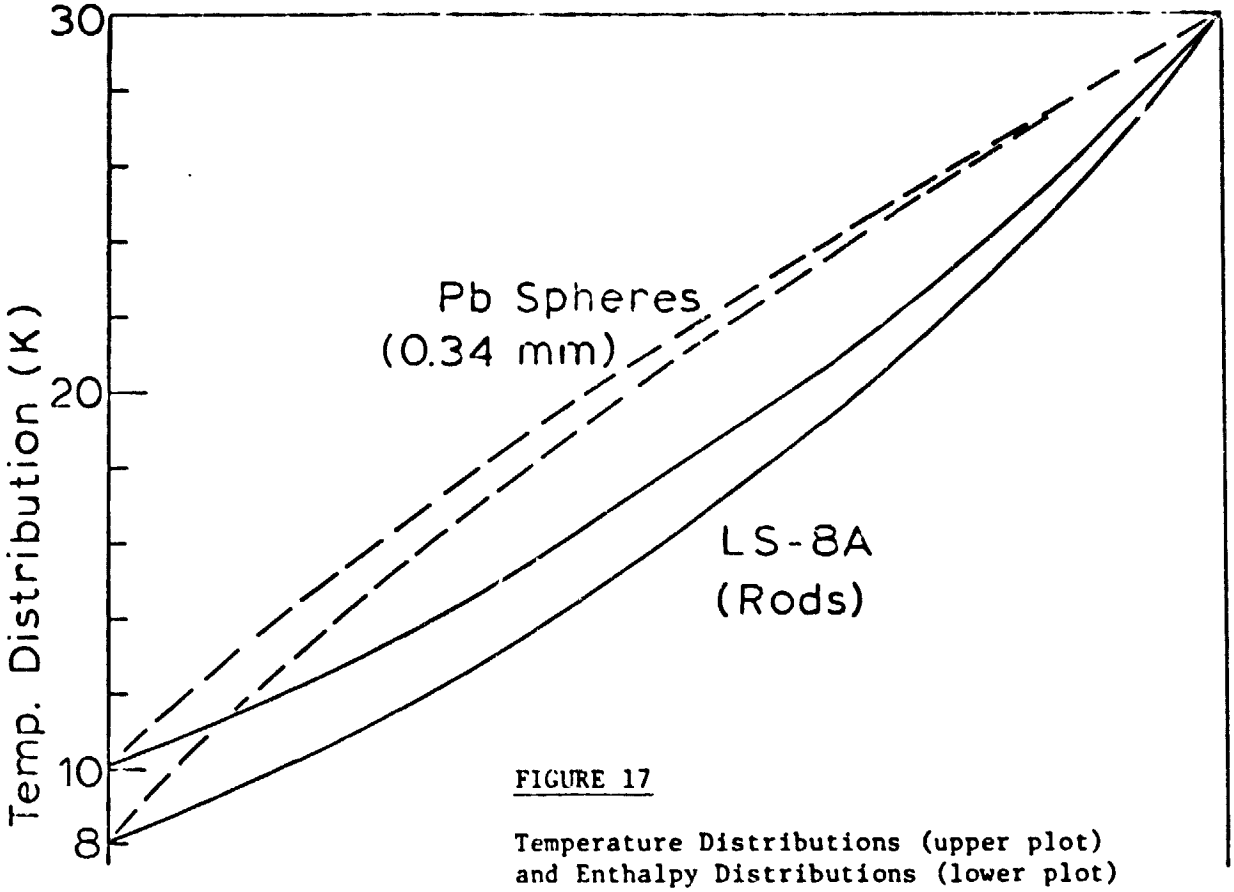

FIGURE 17

Temperature Distributions (upper plot) and Enthalpy Distributions (lower plot) across packed-sphere and packed-rod regenerators.

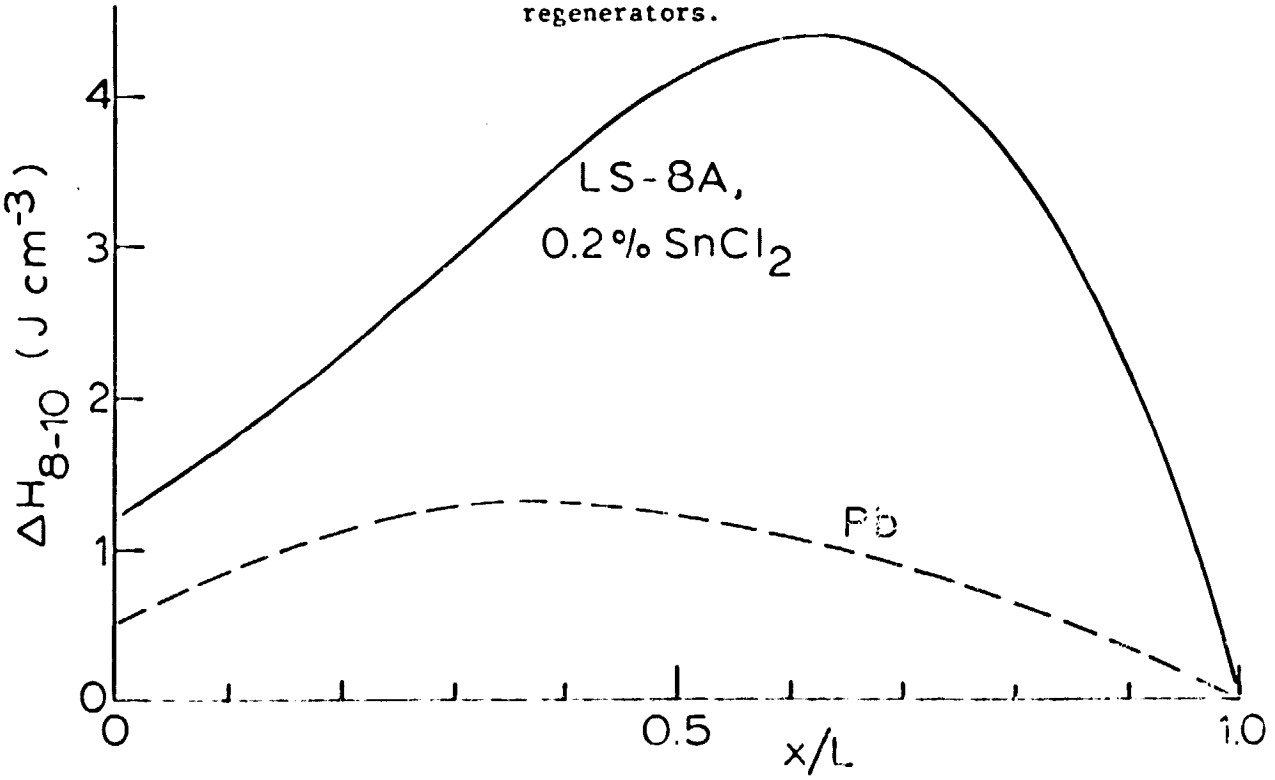

Pb spheres, this maximum occurs at a smaller $x/l = 0.40$ corresponding to $T_1 = 18.56$, $T_2 = 19.37$ K.

Finally, the enthalpy-change data in the lower plot of Fig. 17 are integrated across the regenerator, and the results of these integrations are given in Table III.

Table III

Regenerator Enthalpy Change
($T_H = 30$, $T_{c1} = 8$, $T_{c2} = 10$ K)

Matrix Spheres	$\Delta H(Total)/V$, J cm^{-3} *
Pb, 0.014" diam	0.610
0.2% $SnCl_2$ doped LS-8A	2.033

*V is the total regenerator volume; the results have been corrected for the filling factor for spheres (68%).

This example shows that the optimum LS-8A material theoretically should lead to an improvement of a factor of three in the enthalpy change between a loaded and unloaded regenerator compared to the presently used Pb spheres.

Thermal Equilibration

A concern with potential regenerator materials having large specific heats is the time required for thermal equilibration. That is, if the temperature at the surface of a sphere is instantaneously changed, the sphere will equilibrate to this new temperature in a time given by

$$\tau = 4r^2/\pi^2 k \qquad (7)$$

where r is the sphere radius and k the thermal diffusivity. This is the 99% equilibration time, and $k = K/C$ where K is the thermal conductivity and C the (volumetric) specific heat. Thus, if C is very large, τ can also be very large.

The diffusivity of 0.2% $SnCl_2$-doped LS-8A is derived directly from the data in Figs. 3 and 7, and these data are shown in the upper plot of Fig. 18. The lower plot of Fig. 18 shows the equilibration time estimated from the diffusivity data according to Eq.(7) for three different sphere sizes. Also shown are the He gas dwell times for regenerators operating at 200 and 600 rpm.

The Fig. 18 data show that the optimally-doped LS-8A does not present a thermal equilibration problem for sphere sizes of 0.015" diam or less

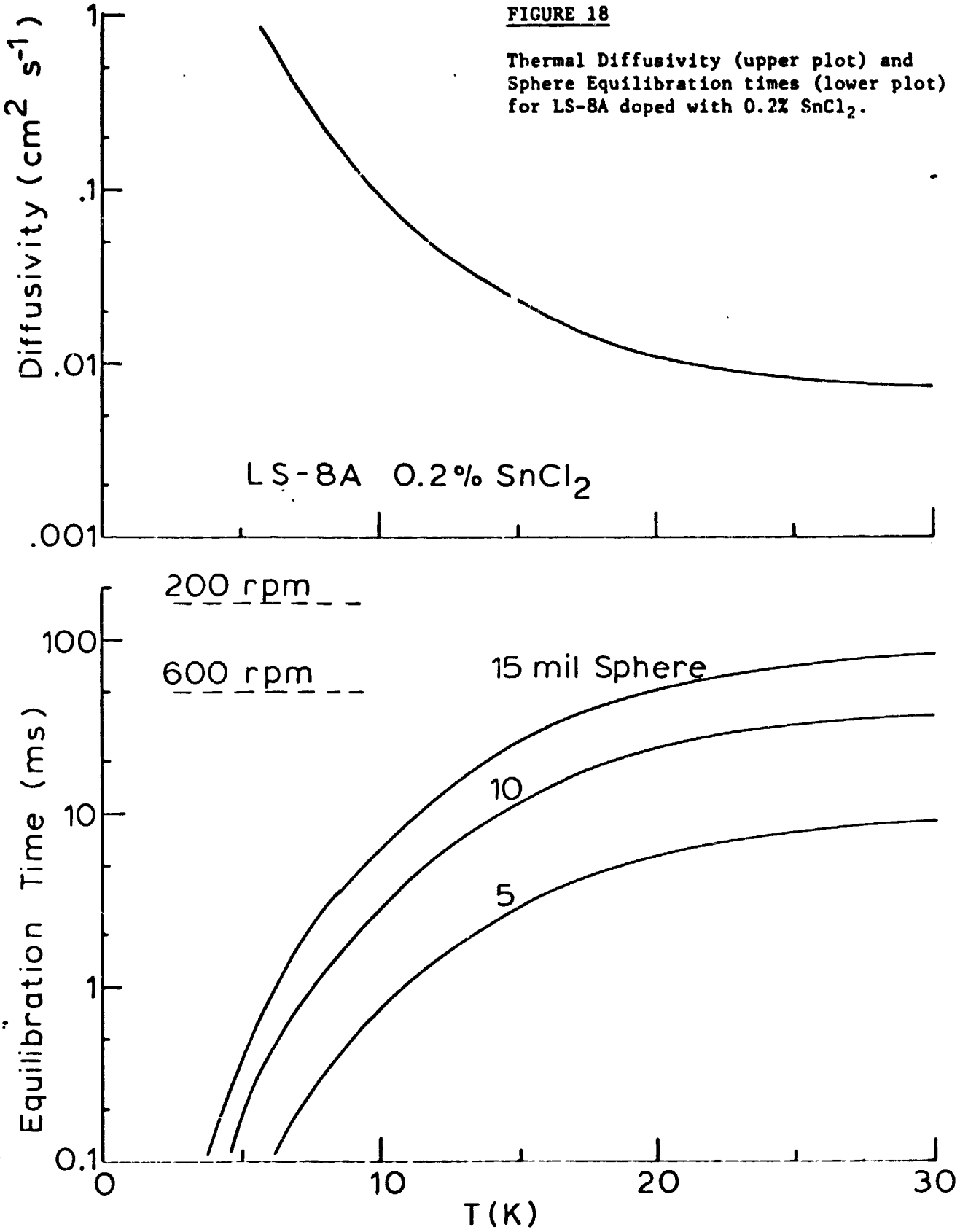

FIGURE 18

Thermal Diffusivity (upper plot) and Sphere Equilibration times (lower plot) for LS-8A doped with 0.2% $SnCl_2$.

for cycle speeds up to 600 rpm. These conclusions are based, of course, on a 99% equilibration time which is quite conservative. We note, moreover, that sphere sizes below 0.015" diam are contemplated for LS-8A and that the trend with cryocoolers is to operate at smaller cycle times than 600 rpm.

VI. CONCLUSIONS

A large amount of experimental data on new materials has been reported in the above, and this program was successful in identifying a new materials' approach to the problem of the regenerator matrix material in cyrocooler applications. What has been firmly established is that:

(1) The LS-8A type materials as a whole are an order of magnitude harder than Pb;

(2) The optimally $SnCl_2$-doped LS-8A has a considerably larger volumetric heat than Pb in the range 3-30 K.

Whether or not the increased hardness of LS-8A will translate into prolonged lifetime of regenerators from the standpoint of sphere pulverization remains to be seen, because pulverization resistance at cryogenic temperatures involves a complex interplay of properties other than hardness (viz., impact resistance, cyclic fatigue, work hardening, and cryogenic embrittlement). Samples of optimally-doped LS-8A spheres, ≈0.012" diam, are being prepared for in site regenerator testing by the Jet Propulsion Laboratory.

The thermodynamic model used here to select the optimum dopant level is appealing because the model incorporates both thermal conductivity and specific heat data. The optimum doping level conveniently falls in that range where $SnCl_2$ is easily incorporated into the LS-8A lattice and leads to improved crystalline perfection. Turning this around, the optimization process may be telling us more about crystalline perfection than anything else.

According to the thermodynamic model, the enthalpy change of the regenerator is theoretically three times larger with optimally-doped LS-8A than with Pb spheres. This is a significant result because this enthalpy change is directly related to the integrated capacity of the regenerator to absorb heat from a load. Therefore, the LS-8A material holds the promise of improving both the reliability and the capacity of the cryocooler.

Along this line, the thermal conductivity curves in Figs. 7 and 16 show that the thermal conductivities of the LS-8A type materials and of a packed column of Pb spheres are about the same order of magnitude, ≈10-20 mW $cm^{-1}K^{-1}$. Remembering that one of the main reasons for using Pb spheres is to reduce the axial thermal conductance means that the LS-8A materials need not be subject to this constraint. In particular, rods of optimally doped LS-8A may ultimately prove to be the best substitution for Pb spheres. There are several compelling reasons for this concept: First, a packed-rod regenerator would obviate the sphere-pulverization problem; second, the packing density for rods is 90.7% compared to 68.0% for spheres, so a 33% increase in the volumetric specific heat is achieved based simply on geometric factors; third, all the thermodynamic advantages and equilibration times developed above for optimally doped LS-8A apply to rods; and fourth, using the thermal conductivity data in Figs. 7 and 16, it can easily be

shown that the packed rods lead to a thermal conductance loss through the regenerator which is 40% of the loss through a packed column of 0.014" diam Pb spheres (this figure is certainly conservative because the conductivity of the Pb spheres is for a freshly packed column and does not reflect the in-use bonding; also, the thermal conductivity of LS-8A rods will certainly be smaller than that of bulk LS-8A, Fig. 7).

A proposal to investigate the use of rods of optimally-doped LS-8A in cryocooler regenerators has been submitted to the Jet Propulsion Laboratory.

Acknowledgements

Dr. Fred Clark of Lake Shore Cryotronics, Inc. offered invaluable assistance in shepherding the computer programs and in helping with the experiments. The Metallurgy Department at Ohio State University graciously made available the microhardness tester.

REFERENCES

[1]See, for example, W. G. Johnston and J. S. Nadeau, ARL report No. 64-135, August 1964.

[2]W. N. Lawless, Cryogenics 15, 273 (1975); Phys. Rev. B14, 134 (1976).

[3]W. N. Lawless, Rev. Sci. Instrum. 48, 361 (1977).

[4]K. T. Aust, A. J. Peat, and J. H. Westbrook, Acta Met. 19, 1469 (1965).

[5]E.S.R. Gopal, Specific Heats at Low Temperatures (Plenum press, New York, 1966).